We are IntechOpen, the world's leading publisher of Open Access books Built by scientists, for scientists

6,900
Open access books available

185,000
International authors and editors

200M
Downloads

Our authors are among the

154
Countries delivered to

TOP 1%
most cited scientists

12.2%
Contributors from top 500 universities



WEB OF SCIENCE™

Selection of our books indexed in the Book Citation Index in Web of Science™ Core Collection (BKCI)

Interested in publishing with us?
Contact book.department@intechopen.com

Numbers displayed above are based on latest data collected.
For more information visit www.intechopen.com



23

Optimal Control Techniques for Spacecraft Attitude Maneuvers

Shifeng Zhang, Shan Qian and Lijun Zhang
National University of Defense Technology, P. R. China

1. Introduction

The capability of attitude maneuvers and attitude tracking for spacecrafts is required in the current sophisticated space missions. In short, it is to obtain command requirements and attitude orientation after some form of control. With the development of space missions, the ability of rapid and energy-saved large-angle attitude maneuvers is actively expected. And the high requirements for the attitude control design system are increasingly demanded. Consequently, optimal control for attitude maneuvers has become an important research direction in the aerospace control area.

From control aspect, spacecraft attitude maneuvers mainly involve trajectory planning (Guidance), attitude determination (Navigation), and attitude control (Control). Further researches about these three key technologies are necessary to achieve optimal control for attitude maneuvers. In this chapter, the necessary background on optimal control for attitude maneuvers of three-axis stabilized spacecraft is provided, and the recent work about guidance and navigation as well as control is summarized, which is presented from three parts as follows:

1. The optimal trajectory planning method for minimal energy maneuvering control problem (MEMCP) of a rigid spacecraft;
2. Attitude determination algorithm based on the improved gyro-drift model;
3. Attitude control of three-axis stabilized spacecraft with momentum wheel system.

2. Optimal trajectory planning method for MEMCP of a rigid spacecraft

The trajectory planning for attitude maneuvers is to determine the standard trajectory for spacecraft attitude maneuvers with multi-constraints using optimization algorithm, which makes the spacecraft move from the initial state to the anticipated state within the specified period and optimizes the given performance index. At present, the optimal trajectory planning problems for spacecraft attitude maneuver mainly focus on the time-optimal and fuel-optimal control. A fuel-optimal reorientation attitude control scheme for symmetrical spacecraft with independent three-axis controls is derived in (Li & Bainum, 1994). Based on the low-thrust gas jet model and Euler's rotational equation of motion, Junkins and Turner (Junkins & Turner, 1980) investigate the optimal attitude control problem with multi-axis maneuvers. They use the closed-form solution of the single-axis maneuver as an initial value and minimize the quadratic sum of the integral of the control torques. Vadali and Junkins (Vadali & Junkins, 1984) have addressed the large-angle reorientation optimal attitude

control problem for asymmetric rigid spacecraft with multiple reaction wheels by using an integral of a weighted quadratic function associated with controlled variables as loss function. Further more, Vadali and Junkins (Vadali & Junkins, 1983) also investigate the optimal attitude maneuvering control problem of rigid vehicles.

The complete optimal attitude control problem is essentially a two-point boundary value problem. Since the input variables of the control system are restricted, Pontryagin's Minimum Principle (PMP) is usually used to solve the optimal attitude control problem of the symmetric or asymmetric rigid spacecraft with constraints. The optimal attitude control problem with fixed maneuvering period has been solved in (Vadali & Junkins, 1984; Vadali & Junkins, 1983; Dwyer, 1982; Schaub & Junkins, 1997). In practice, numerical methods are generally used to solve the highly nonlinear and close coupling differential equations derived from PMP. However, the method falls short to deal with dynamic optimization problem with uncertain terminal time, and the shooting method is commonly adopted whereas it will increase the iterations and computational burden. Therefore, the satisfied development has not yet been achieved for large-angle attitude reorientation of asymmetric rigid spacecraft up to now.

Recently, (Chung & Wu, 1992) presents a nonlinear programming (NLP) method to solve time-optimal control problem for linear system. Different from the conventional shooting method which sets the time step as a fixed value, the NLP method considers the time step as a variable and obtains the optimal solution on the premise of ensuring sufficient discretization precision of the model. (Yang et al., 2007) further discusses MEMCP of a rigid spacecraft, which introduces two aspects of research on the three-axis spacecraft with limited output torque, including: 1) the description of MEMCP using NLP method, and 2) the construction method for initial feasible solution of the NLP. However, the derivation in that paper has some errors and the initial feasible solution does not conform to the actual motion of the spacecraft. Moreover, the method augments the optimizing time and the randomness of the variation between the adjacent attitude commands. Consequently, this section (Zhang et al., 2009) further improves the proposed method and presents a new construction method for initial feasible solution of the NLP, and obtains the optimal control period and torques by the energy-optimal criterion. Simulation results demonstrate the feasibility and advantages of the improved method.

2.1 Dynamical and kinematical equations of a rigid spacecraft

The attitude motion of a spacecraft can be described by its dynamical and kinematical equations. In general, the dynamic equation of motion can be represented as

$$\begin{bmatrix}\dot{\omega}_x\\ \dot{\omega}_y\\ \dot{\omega}_z\end{bmatrix} = -\begin{bmatrix}1/I_x & 0 & 0\\ 0 & 1/I_y & 0\\ 0 & 0 & 1/I_z\end{bmatrix}\left\{\begin{bmatrix}0 & -\omega_z & \omega_y\\ \omega_z & 0 & -\omega_x\\ -\omega_y & \omega_x & 0\end{bmatrix}\times\left\{\begin{bmatrix}(I_x+I_1)\omega_x\\ (I_y+I_2)\omega_y\\ (I_z+I_3)\omega_z\end{bmatrix}+\begin{bmatrix}I_1\omega_1\\ I_2\omega_2\\ I_3\omega_3\end{bmatrix}\right\}\right\}-\begin{bmatrix}T_1/I_x\\ T_2/I_y\\ T_3/I_z\end{bmatrix} \quad (1)$$

where I_x, I_y, I_z and I_1, I_2, I_3 denote the moment of inertia of rigid spacecraft about the principal axis and the three reaction wheels, respectively. $\omega_x, \omega_y, \omega_z$ are the components of spacecraft's angular velocity expressed in its body-fixed frame, and $\omega_1, \omega_2, \omega_3$ are the components of the reaction wheel's angular velocity. T_1, T_2, T_3 are the control torques provided by the perpendicular momentum wheels along the principal axis.

The equation of angular motion of the momentum wheels can be obtained from Eq.(1)

$$\begin{bmatrix}\dot{\omega}_1\\ \dot{\omega}_2\\ \dot{\omega}_3\end{bmatrix}=\begin{bmatrix}1/I_x & 0 & 0\\ 0 & 1/I_y & 0\\ 0 & 0 & 1/I_z\end{bmatrix}\begin{bmatrix}0 & -\omega_z & \omega_y\\ \omega_z & 0 & -\omega_x\\ -\omega_y & \omega_x & 0\end{bmatrix}\times\left\{\begin{bmatrix}(I_x+I_1)\omega_x\\ (I_y+I_2)\omega_y\\ (I_z+I_3)\omega_z\end{bmatrix}+\begin{bmatrix}I_1\omega_1\\ I_2\omega_2\\ I_3\omega_3\end{bmatrix}\right\}+\begin{bmatrix}(1/I_x+1/I_1)T_1\\ (1/I_y+1/I_2)T_2\\ (1/I_z+1/I_3)T_3\end{bmatrix} \quad (2)$$

Considering the 1-2-3 sequence of rotations, the kinematic equation of motion using Euler angle representation is given by

$$\begin{bmatrix}\dot{\phi}\\ \dot{\theta}\\ \dot{\psi}\end{bmatrix}=\begin{bmatrix}\sec\theta\cos\psi & -\sec\theta\sin\psi & 0\\ \sin\psi & \cos\psi & 0\\ -\tan\theta\cos\psi & \tan\theta\sin\psi & 1\end{bmatrix}\begin{bmatrix}\omega_x\\ \omega_y\\ \omega_z\end{bmatrix} \quad (3)$$

where φ is roll angle, θ is pitch angle and ψ is yaw angle.

2.2 Modeling and analysis of MEMCP

The MEMCP of the rigid spacecraft between two attitudes can be described as an optimizing problem as follows.

The initial attitude is given by

$$\begin{cases}(\phi(0),\theta(0),\psi(0))=(\phi_{\text{initial}},\theta_{\text{initial}},\psi_{\text{initial}})\\ (\omega_x(0),\omega_y(0),\omega_z(0))=(0,0,0)\\ (\omega_1(0),\omega_2(0),\omega_3(0))=(\omega_{1,\text{initial}},\omega_{2,\text{initial}},\omega_{3,\text{initial}})\end{cases} \quad (4)$$

The goal is to determine the control inputs $\boldsymbol{T}(t)=[T_1(t),T_2(t),T_3(t)]^{\mathrm{T}}$ for some $t\in[0,t_f]$ to minimize the following objective function

$$J=\int_0^{t_f}(T_1^2(t)+T_2^2(t)+T_3^2(t))dt=\int_0^{t_f}\sum_{k=1}^{3}T_k^2(t)dt$$

subject to

$$\begin{aligned}&(\phi(t_f),\theta(t_f),\psi(t_f))=(\phi_{\text{final}},\theta_{\text{final}},\psi_{\text{final}})\\ &(\omega_x(t_f),\omega_y(t_f),\omega_z(t_f))=(0,0,0)\\ &T_{i,\min}\le T_i(t)\le T_{i,\max},\ \text{for}\ t\in[0,t_f],\quad i=1,2,3\end{aligned} \quad (5)$$

where $(\phi_{\text{initial}},\theta_{\text{initial}},\psi_{\text{initial}})$ and $(\phi_{\text{final}},\theta_{\text{final}},\psi_{\text{final}})$ represent the initial and desired final attitudes of the spacecraft, respectively. t_f is determined by the optimization process.

Due to the characteristics of highly nonlinear and close coupling of the problem, it will be solved in the discrete-time domain using numerical method. First, we divide the interval $t\in[0,t_f]$ into N equidistant subinterval and assume that the angular acceleration is constant in each subinterval. Therefore, from Eq.(1) and Eq.(2), we can obtain

$$\begin{bmatrix}\omega_x(i)\\ \omega_y(i)\\ \omega_z(i)\end{bmatrix}=\begin{bmatrix}\omega_x(0)\\ \omega_y(0)\\ \omega_z(0)\end{bmatrix}-\begin{bmatrix}1/I_x & 0 & 0\\ 0 & 1/I_y & 0\\ 0 & 0 & 1/I_z\end{bmatrix}\sum_{k=0}^{i-1}\left\{\begin{bmatrix}0 & -\omega_z(k) & \omega_y(k)\\ \omega_z(k) & 0 & -\omega_x(k)\\ -\omega_y(k) & \omega_x(k) & 0\end{bmatrix}\times\right.$$
$$\left.\begin{bmatrix}(I_x+I_1)\omega_x(k)+I_1\omega_1(k)\\ (I_y+I_2)\omega_y(k)+I_2\omega_2(k)\\ (I_z+I_3)\omega_z(k)+I_3\omega_3(k)\end{bmatrix}+\begin{bmatrix}T_1(k)/I_x\\ T_2(k)/I_y\\ T_3(k)/I_z\end{bmatrix}\right\}\Delta t \tag{6}$$

$$\begin{bmatrix}\omega_1(i)\\ \omega_2(i)\\ \omega_3(i)\end{bmatrix}=\begin{bmatrix}\omega_1(0)\\ \omega_2(0)\\ \omega_3(0)\end{bmatrix}+\begin{bmatrix}1/I_x & 0 & 0\\ 0 & 1/I_y & 0\\ 0 & 0 & 1/I_z\end{bmatrix}\sum_{k=0}^{i-1}\left\{\begin{bmatrix}0 & -\omega_z(k) & \omega_y(k)\\ \omega_z(k) & 0 & -\omega_x(k)\\ -\omega_y(k) & \omega_x(k) & 0\end{bmatrix}\times\right.$$
$$\left.\begin{bmatrix}(I_x+I_1)\omega_x(k)+I_1\omega_1(k)\\ (I_y+I_2)\omega_y(k)+I_2\omega_2(k)\\ (I_z+I_3)\omega_z(k)+I_3\omega_3(k)\end{bmatrix}+\begin{bmatrix}(1/I_x+1/I_1)T_1(k)\\ (1/I_y+1/I_2)T_2(k)\\ (1/I_z+1/I_3)T_3(k)\end{bmatrix}\right\}\Delta t \tag{7}$$

where $\Delta t=t_i-t_{i-1}=t_f/N$, $i=1,2,\cdots,N$.

Suppose that the time derivative of ϕ, θ, ψ are constant during each subinterval, then we have

$$\begin{bmatrix}\phi(i)\\ \theta(i)\\ \psi(i)\end{bmatrix}=\begin{bmatrix}\phi(0)\\ \theta(0)\\ \psi(0)\end{bmatrix}+\sum_{k=0}^{i-1}\begin{bmatrix}\sec\theta(k)\cos\psi(k) & -\sec\theta(k)\sin\psi(k) & 0\\ \sin\psi(k) & \cos\psi(k) & 0\\ -\tan\theta(k)\cos\psi(k) & \tan\theta(k)\sin\psi(k) & 1\end{bmatrix}\begin{bmatrix}\omega_x(k)\\ \omega_y(k)\\ \omega_z(k)\end{bmatrix}\Delta t \tag{8}$$

Therefore, the previous MEMCP can be described as a constrained NLP problem. Given the initial attitudes, determine the values of $\boldsymbol{T}(0),\cdots,\boldsymbol{T}(N-1)$ and Δt to minimize

$$J=\sum_{k=1}^{3}\sum_{i=0}^{N-1}T_k^2(i)\Delta t$$

subject to

$$\begin{cases}0<\varepsilon<\Delta t<\Delta t_{\text{upper}}\\ (\phi(N),\theta(N),\psi(N))=(\phi_{\text{final}},\theta_{\text{final}},\psi_{\text{final}})\\ (\omega_x(N),\omega_y(N),\omega_z(N))=(0,0,0)\\ T_{i,\min}\le T_i(j)\le T_{i,\max},\ \ i=1,2,3;\ \ j=0,1,\cdots,N-1\end{cases} \tag{9}$$

where ε is a small positive number to ensure the computation time is not excessively long. The question is how to select the value of N to solve the discrete NLP problem mentioned above. For the unconstrained linear programming problem, (Chung & Wu, 1992) points out the initial value of N must be greater than the dimensions of the state variables, which is adopted in this paper.

2.3 Construction of initial feasible solution of NLP problem

The NLP problem usually requires the initial feasible solution to start the optimization process. The initial feasible solution is a set of optimization variables $\boldsymbol{T}(0),\cdots,\boldsymbol{T}(N-1)$ and Δt which satisfy Eq.(9). Different initial feasible solutions will yield different local optimal solutions, and the deviation of the initial feasible solution from the optimal solution will affect the iteration times and computation time. (Yang et al., 2007) presents a construction method of the initial feasible solution. However, the solution does not agree well with the actual motion of the spacecraft, and the randomness of variation between the adjacent attitude commands is excessively large. To solve this problem, a new construction of the initial feasible is presented in this section.

The first step is to determine a maneuvering trajectory satisfying the boundary conditions without the constraints of the control torques. Then, the set of control torques computed in the above trajectory is checked. If it satisfies all the constraints, the set of control torques and Δt is the initial feasible solution. Otherwise, we need to adjust the velocity and acceleration until finding a set of initial feasible solution.

With the given N, the attitude trajectories satisfying the boundary conditions can be determined by

$$\phi(i)=\begin{cases}\phi_{\text{initial}} & i=0,1\\ \gamma_i\phi(i-1)+\dfrac{i-2}{N-2}\gamma_i\left(\phi_{\text{final}}-\phi(i-1)\right) & i=2,\cdots,N-1\\ \phi_{\text{final}} & i=N,N+1\end{cases}\quad \theta(i)=\begin{cases}\theta_{\text{initial}} & i=0,1\\ \theta(i-1)+\dfrac{i-2}{N-2}\gamma_i\left(\theta_{\text{final}}-\theta(i-1)\right) & i=2,\cdots,N-1\\ \theta_{\text{final}} & i=N,N+1\end{cases}$$

$$\psi(i)=\begin{cases}\psi_{\text{initial}} & i=0,1\\ \psi(i-1)+\dfrac{i-2}{N-2}\gamma_i\left(\psi_{\text{final}}-\psi(i-1)\right) & i=2,\cdots,N-1\\ \psi_{\text{final}} & i=N,N+1\end{cases} \tag{10}$$

where γ_i is a random number obeying the uniform distribution in the interval $[0,1]$. Euler angle vector is defined as $\boldsymbol{\lambda}=[\phi,\theta,\psi]^{\mathrm{T}}$, and it is obvious that $\boldsymbol{\lambda}(i)$ satisfies the initial constraints in Eq.(4) and final constraints in Eq.(9).

Take the roll angle ϕ for example, we can easily obtain the inequalities $\phi(i-1)\le\phi(i)\le\phi_{final}$ or $\phi(i-1)\ge\phi(i)\ge\phi_{final}$. It is shown that the attitude trajectory $\phi(i)$ constructed by the previous model approaches the value of ϕ_{final} all along. The process is not reciprocating and in well agreement with the optimal maneuvering process.

Choose the appropriate value of Δt to satisfy the constraint $0<\varepsilon<\Delta t<\Delta t_{\text{upper}}$, so that

$$\begin{bmatrix}\dot\phi(i)\\ \dot\theta(i)\\ \dot\psi(i)\end{bmatrix}=\begin{bmatrix}\dfrac{\phi(i+1)-\phi(i)}{\Delta t}\\ \dfrac{\theta(i+1)-\theta(i)}{\Delta t}\\ \dfrac{\psi(i+1)-\psi(i)}{\Delta t}\end{bmatrix}\qquad i=0,1,\cdots,N \tag{11}$$

where $[\dot{\phi}(0) \quad \dot{\theta}(0) \quad \dot{\psi}(0)] = [0 \quad 0 \quad 0]$ and $[\dot{\phi}(N) \quad \dot{\theta}(N) \quad \dot{\psi}(N)] = [0 \quad 0 \quad 0]$. We can obtain from Eq.(3) that

$$\begin{bmatrix} \omega_x(i) \\ \omega_y(i) \\ \omega_z(i) \end{bmatrix} = \begin{bmatrix} \sec\theta(i)\cos\psi(i) & -\sec\theta(i)\sin\psi(i) & 0 \\ \sin\psi(i) & \cos\psi(i) & 0 \\ -\tan\theta(i)\cos\psi(i) & \tan\theta(i)\sin\psi(i) & 1 \end{bmatrix}^{-1} \begin{bmatrix} \dot{\phi}(i) \\ \dot{\theta}(i) \\ \dot{\psi}(i) \end{bmatrix} \tag{12}$$

Obviously, the angular velocity $\boldsymbol{\omega}$ also satisfies the boundary constraints in Eq.(4) and Eq.(9).

Then let us check whether the maneuvering trajectory satisfies the torque constraints or not. After determining $(\omega_x(i), \omega_y(i), \omega_z(i))$ and $(\dot{\omega}_x(i), \dot{\omega}_y(i), \dot{\omega}_z(i))$, the corresponding values of $\boldsymbol{T}(0), \cdots, \boldsymbol{T}(N-1)$ can be sequentially calculated. The calculation flow is summarized as follows:

1. Substituting $(\omega_1(0), \omega_2(0), \omega_3(0))$ and $(\omega_x(0), \omega_y(0), \omega_z(0))$ into Eq.(6) to calculate $(T_1(0), T_2(0), T_3(0))$.
2. Substituting $(\omega_1(0), \omega_2(0), \omega_3(0))$, $(\omega_x(0), \omega_y(0), \omega_z(0))$ and $(T_1(0), T_2(0), T_3(0))$ into Eq.(7) to determine $(\omega_1(1), \omega_2(1), \omega_3(1))$.
3. Repeat the step 1 and step 2, and determine the values of $\boldsymbol{T}(0), \cdots, \boldsymbol{T}(N-1)$ sequentially.

If the obtained control torques satisfy the constraints, the set of $\boldsymbol{T}(0), \cdots, \boldsymbol{T}(N-1)$ and Δt is the initial feasible solution. Otherwise, Δt is increased to decrease the maneuvering velocity and acceleration until the control torques satisfy the constraints. Since the initial feasible solution is stochastically yielded via Eq.(10), the final optimal control scheme is derived from the multiple initial feasible solutions separately.

2.4 NLP solution process of MEMCP

On the basis of the previous sections, the NLP solution process of MEMCP can be described as follows:

Step 1. Choose an integer N and iteration number n_f;
Step 2. Set $i = 0$;
Step 3. Describe the MEMCP using NLP model;
Step 4. $i = i + 1$;
Step 5. Determine the NLP initial feasible solution of MEMCP;
Step 6. Solve the MEMCP using NLP with the given initial values;
Step 7. If $i \le n_f$, then go to step 5, if not, continue;
Step 8. Choose the smallest local optimal solution as the solution of MEMCP;
Step 9. End.

In the above algorithm, the computation time and nonlinear degree should be considered to choose n_f, it is generally set as 20. In addition, the value of Δt is required smaller to obtain the high discretization accuracy, while it is also required as larger as possible to minimize the energy consumption. By the tradeoff, we can determine the upper limit denoted as Δt_{limit}. If $\Delta t(N)$ is greater than Δt_{limit}, the value of N needs to be adjusted. (Chung & Wu, 1992) provides a selection and adjustment approach about the values of Δt_{limit} and N.

2.5 Simulation results

In this section, the feasibility and validity of the above approach are verified. The following parameters are used for simulations. The initial conditions are $(\omega_x(0),\omega_y(0),\omega_z(0))=(0,0,0)$, $(\phi(0),\theta(0),\psi(0))=(0,0,0)$, $(\omega_1(0),\omega_2(0),\omega_3(0))=(0,0,0)$,and the final conditions are: $(\omega_x(t_f),\omega_y(t_f),\omega_z(t_f))=(0,0,0)$, $(\phi(t_f),\theta(t_f),\psi(t_f))=(30,45,0)$ .The boundary conditions of control torques are :

$(T_{1,\max},T_{2,\max},T_{3,\max})=(0.56,0.53,0.24)(\text{Nm})$, $(T_{1,\min},T_{2,\min},T_{3,\min})=(-0.56,-0.53,-0.24)(\text{Nm})$ .The moment of inertia of spacecraft are $(I_x,I_y,I_z)=(182,329,336)(\text{kgm}^2)$, and the moment of inertia of momentum wheels are $I_1=I_2=I_3=0.041(\text{kgm}^2)$.

2.5.1 Case 1

The case is used to verify the construction of initial feasible solution of NLP. When Δt is small (e.g., $\Delta t=6s$), the initial set of control torques $\boldsymbol{T}(0),\cdots,\boldsymbol{T}(N-1)$ is large. The control torques obtained will be easy to exceed the constraints, as shown in Table 1. It is necessary to increase the value of Δt (e.g., $\Delta t=10s$) to decrease the maneuvering velocity and acceleration. Thus, the control torques can satisfy the constraints, as illustrated in Table 2.

	ϕ	θ	ψ	T_1	T_2	T_3
1	0	0	0	-0.272	-0.737	0
2	3.080	0	0	0.009	0.021	-0.039
3	6.073	4.620	0	-0.218	-0.605	-0.103
4	11.60	9.110	0	-0.133	-0.423	-0.213
5	18.88	17.39	0	0.116	0.211	-0.140
6	25.29	28.32	0	0.316	0.908	0.234
7	27. 90	37.93	0	0.160	0.547	0.226
8	28.22	41.85	0	-0.026	-0.095	-0.044
9	28.94	42.33	0	-0.021	-0.080	-0.040
10	30	43.41	0	0.068	0.253	0.118
11	30	45	0	--	--	--

Table 1. A set of infeasible solution to $\Delta t=6s$ and $N=10$

	ϕ	θ	ψ	T_1	T_2	T_3
1	0	0	0	-0.113	-0.307	0
2	0	0	0	0.065	0.175	-0.008
3	3.563	5.345	0	-0.130	-0.357	-0.036
4	5.091	7.636	0	0.036	0.086	-0.032
5	10.76	16.14	0	-0.094	-0.296	-0.111
6	15.44	23.15	0	0.141	0.381	0.062
7	23.55	35.32	0	0.069	0.223	0.083
8	27.24	40.85	0	0.026	0.092	0.041
9	28.34	42.51	0	-0.037	-0.138	-0.063
10	28.37	42.56	0	0.038	0.140	0.065
11	30	45	0	--	--	--

Table 2. A set of feasible solution to $\Delta t=10s$ and $N=10$

2.5.2 Case 2

Fig. 1 illustrates the performance index J with respect to different values of Δt_{upper} in the cases of $N = 10$ and $N = 20$. When the maneuvering times N is fixed, we can find that a larger value of Δt_{upper} will result in a smaller value of J; when Δt_{upper} is fixed, the greater value of N will result in the smaller value of performance index J. It is shown that the longer maneuvering period will require the smaller energy consumption which agrees well with the actual situation.

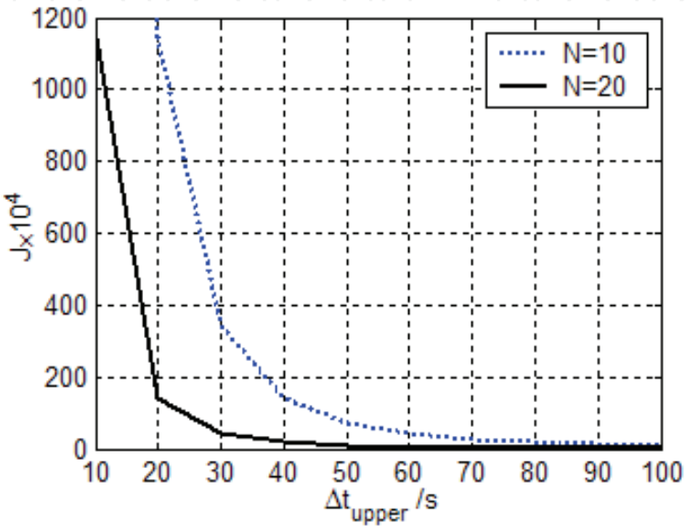


Fig. 1. Performance index J with respect to Δt_{upper}

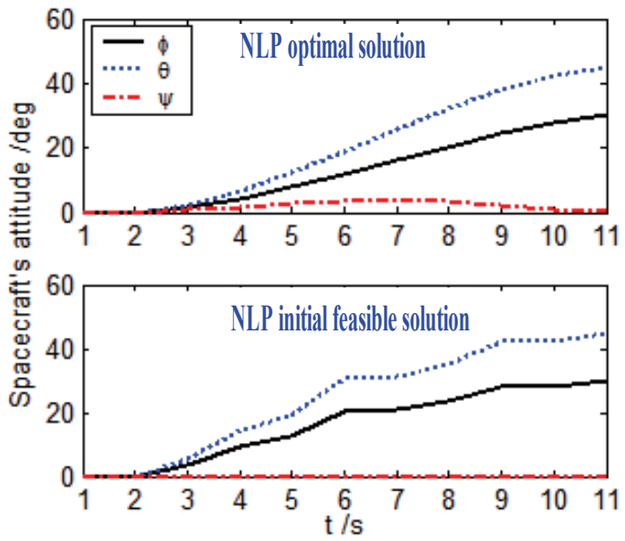


Fig. 2. Spacecraft's attitude

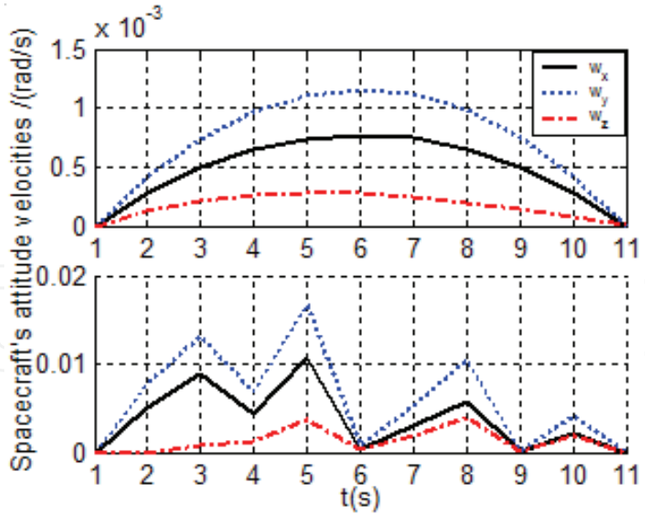


Fig. 3. Spacecraft's angular velocities

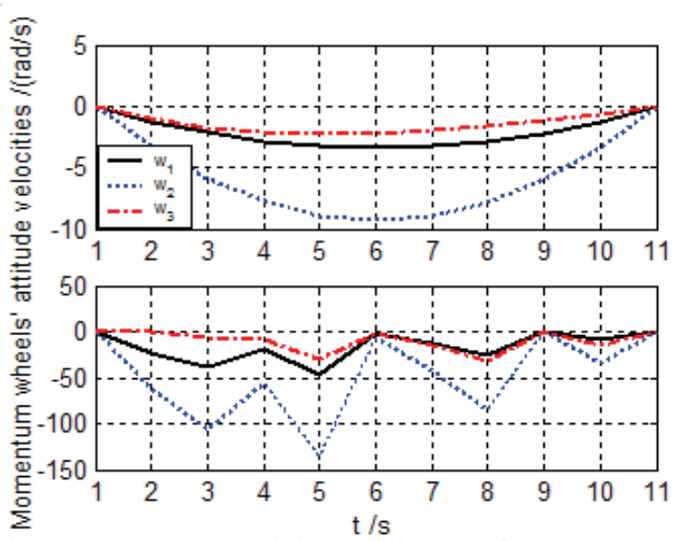


Fig. 4. Momentum wheels' angular velocities

2.5.3 Case 3

In this simulation case, we choose the parameters $N = 10$ and Δt_{upper}=100s . Figs. 2-4 show the responses of attitude angle $\boldsymbol{\lambda}$ and angular velocities of spacecraft $\boldsymbol{\omega}$ as well as angular velocity of momentum wheels $\boldsymbol{\omega}_w$, respectively. In each figure, we compared the results in the case of NLP initial feasible solution (top) and NLP optimal solution (bottom). Obviously, in the initial feasible solution of NLP, the Euler angles $\boldsymbol{\lambda}$ tend to the final attitude angle all the time while the variation curve is not smooth. The curve of $\boldsymbol{\omega}_w$ is oscillating and unstable, which means that the control inputs vary severely during the attitude maneuvers. After a period of the NLP optimizing, Euler angle $\boldsymbol{\lambda}$ approaches the desired states gradually, control curve $\boldsymbol{\omega}_w$ is steady and smooth, and the energy function of the control decreases from 7.3217 to 9.1401×10^{-4}.

3. Attitude determination algorithm based on the improved gyro-drift model

Attitude determination is the process of computing the orientation of the spacecraft relative to an inertial reference frame or some reference objects in space (e.g., Earth, Sun, Star) using attitude sensors. It is prerequisite of attitude maneuvering control for spacecraft.

For a three-axis stabilized spacecraft, the attitude measurement system consisting of gyroscopes and star sensors is the typical composition of attitude determination. Based on the attitude kinematical equations of spacecraft, combined with Extend Kalman Filter (EKF) algorithm, the attitude can be estimated and the accumulated errors of gyroscopes can be eliminated using star sensor data. Modeling the gyro drift is required for the process and zero-order or one-order Markovian model is usually adopted. When adopting the above gyro drift model, the filter has good performance and fast rate of convergence. However, the estimated error curves of attitude and angular velocity are not smooth with various noises and the maximum relative error can reache to 10%. Since attitude and angular velocity are the feedback signals in the attitude control system (ACS), the unstable estimated errors may affect the stability and precision of the control system. For this problem, two types of improved gyro drift models are presented to decrease the steady state deviation of estimated errors and improve the estimated accuracy (Qian et al., 2009).

3.1 Gyro-based attitude determination scheme

3.1.1 Fundamental principle

In the gyro-based attitude determination system, the gyro data provide a continuous attitude reference through attitude propagation, but the estimated attitude errors accumulate due to the gyro drift. Star sensor data provide high-precision attitude information to eliminate the errors at some sampling rate, thereby data processing is indispensable owing to the measurement errors. Therefore, the attitude filter can be established using the gyroscope and star sensor data, where the Extended Kalman filter algorithm is used to estimate and correct the attitude.

3.1.2 State equation of attitude determination system

The gyro-based determination scheme includes prediction estimation and observation correction. Corresponding attitude estimation model includes the state prediction model and state-error estimation model.

The orbital coordinate system is selected as the reference frame of the attitude motion of the spacecraft, and the state equations of the attitude determination system can be represented as (Wertz, 1998)

$$\dot{\mathbf{q}} = \frac{1}{2}\Omega\left(\boldsymbol{\omega}_{ob}^{b}\right)\mathbf{q} \tag{13}$$

$$\dot{\mathbf{b}} = \mathbf{v}_b \tag{14}$$

where $\mathbf{q} \equiv [q_1 \ \boldsymbol{q}_{24}^{\mathrm{T}}]^{\mathrm{T}}$ denotes orbital-to-body attitude quaternion, $\boldsymbol{\omega}_{ob}^{b}$ denotes the angular velocity in the orbital coordinate system determined by $\omega_{ob}^{b} = \omega - R_o^b(\mathrm{q}) \cdot \omega_{io}^{o}$, ω denotes the inertial angular velocity measured by the gyroscope, $\omega = \mathrm{U} - \mathrm{b} - \mathrm{v}_g$; R_o^b is the orbital-to-

body attitude matrix, ω_{io}^{o} denotes the orbital angular velocity with respect to inertial space. $\boldsymbol{b}$ is the drift-rate bias and v_g is the drift-rate noise.

1. State prediction model

Integrating the Eq.(13) the attitude quaternion estimates in the interval $[t-\Delta t_g,\ \ t]$ can be obtained, and the prediction model of state estimation is given by

$$\hat{\mathrm{q}}(t)=\hat{\mathrm{q}}\left(t-\Delta t_g\right)+\frac{1}{2}\Omega\left(\hat{\boldsymbol{\omega}}_{ob}^{b}\cdot\Delta t_g\right)\hat{\mathrm{q}}\left(t-\Delta t_g\right) \tag{15}$$

$$\hat{\mathrm{b}}(t)=\hat{\mathrm{b}}\left(t-\Delta t_g\right) \tag{16}$$

where superscript " $\wedge$ " denotes the estimates of the corresponding value.

2. Error state equation

The error state equation of the error quaternion can be given by (Wang, 2004)

$$\begin{cases}\Delta\dot{q}_1=0\\ \Delta\dot{\mathrm{q}}_{24}=-[\hat{\omega}\times]\Delta\mathrm{q}_{24}-\dfrac{1}{2}\Delta\mathrm{b}-\dfrac{1}{2}\mathrm{v}_g\\ \Delta\dot{\mathrm{b}}=\mathrm{v}_b\end{cases} \tag{17}$$

where $\Delta\mathrm{q}\equiv[\Delta q_1\ \Delta\mathrm{q}_{24}^{\mathrm{T}}]^{\mathrm{T}}$ denotes the attitude error quaternion, and $\Delta\mathrm{b}=\mathrm{b}-\hat{\mathrm{b}}$.

3.1.3 Observation model

Observation model 1: When gyroscope and star sensor are adopted as the sensors for the attitude determination system, the error state vector is defined as $\delta\mathrm{X}\equiv\left[\Delta q_2\ \Delta q_3\ \Delta q_4\ \Delta q_1\ \Delta b_1\ \Delta b_2\ \Delta b_3\right]^{\mathrm{T}}$, and the observation vector is observation residuals of the star sensor defined as $\mathrm{Z}\equiv\left[\Delta\varphi\ \ \Delta\theta\ \ \Delta\psi\right]^{T}$. With the small angle approximations, the observation equation can be given by

$$\mathrm{Z}_k=\boldsymbol{H}_k\cdot\delta\mathrm{X}_k+\mathrm{V}_k \tag{18}$$

with

$$\begin{bmatrix}\Delta\varphi\\ \Delta\theta\\ \Delta\psi\end{bmatrix}=\begin{bmatrix}\varphi_m\\ \theta_m\\ \psi_m\end{bmatrix}-\begin{bmatrix}\hat{\varphi}\\ \hat{\theta}\\ \hat{\psi}\end{bmatrix}$$

where $[\hat{\varphi}\ \ \hat{\theta}\ \ \hat{\psi}]^{\mathrm{T}}$ is the attitude estimate derived from the prediction model, and the observation matrix is $\boldsymbol{H}_k=\left[2\boldsymbol{I}_{3\times3}\ \ \boldsymbol{0}_{3\times3}\right]$.

Observation model 2: When the attitude sensors for the attitude determination system are chosen as gyroscope and sun sensor as well as infrared horizon sensor, the constant biases along roll axis and pitch axis of the infrared horizon senor are generally augmented into the state variable. Therefore, we choose the state vector as $\mathrm{X}\equiv[\mathrm{q}^{\mathrm{T}}(t)\ \ \mathrm{b}^{\mathrm{T}}(t)\ \varphi_{bias}\ \theta_{bias}]^{\mathrm{T}}$ and

error state vector as $\delta \mathrm{X} \equiv \left[\Delta q_2\ \Delta q_3\ \Delta q_4\ \Delta q_1\ \Delta b_1\ \Delta b_2\ \Delta b_3\ \Delta\varphi_{bias}\ \Delta\theta_{bias}\right]^{\mathrm{T}}$. Observation vector is the observation residuals between infrared horizon sensor and sun sensor, denoted as $\mathrm{Z}_k \equiv [\Delta\varphi\ \Delta\theta\ \Delta D_\xi\ \Delta D_\eta]^{\mathrm{T}}$. Similarly, the observation equation is given by

$$\mathrm{Z}_k = \boldsymbol{H}_k \cdot \delta \mathrm{X}_k + \mathrm{V}_k \tag{19}$$

with

$$\begin{bmatrix}\Delta\varphi \\ \Delta\theta\end{bmatrix} = \left(\begin{bmatrix}\varphi_m \\ \theta_m\end{bmatrix} - \begin{bmatrix}\hat{\varphi}_{bias} \\ \hat{\theta}_{bias}\end{bmatrix}\right) - \begin{bmatrix}\hat{\varphi} \\ \hat{\theta}\end{bmatrix}$$

$$\begin{bmatrix}\Delta D_\xi \\ \Delta D_\eta\end{bmatrix} = \begin{bmatrix}D_{\xi m} \\ D_{\eta m}\end{bmatrix} - \begin{bmatrix}\hat{D}_\xi \\ \hat{D}_\eta\end{bmatrix}$$

where $\hat{\varphi}_{bias}$ and $\hat{\theta}_{bias}$ represent the bias error estimates along the roll and pitch axes of the infrared horizon sensor, respectively. $[D_{\xi m}\ D_{\eta m}]^{\mathrm{T}}$ and $[\hat{D}_\xi\ \hat{D}_\eta]^{\mathrm{T}}$ represent the measurements from Sun sensor and corresponding estimates, respectively.

3.2 Improved gyro drift model

Improved gyro model 1: Error quaternion $\Delta\mathrm{q}$ is introduced into the gyro drift model (Thienel, 2004), that is

$$\Delta\dot{\mathrm{b}} = \frac{\alpha}{2} \cdot \Delta \mathrm{q}_{24} \cdot sign(\Delta q_1) + \mathrm{v}_b \tag{20}$$

where α is a positive scale factor, $sign(\cdot)$ is sign function.

The above gyro drift model makes good use of the observability of $\Delta\mathrm{q}$ and associates $\Delta\mathrm{q}$ with gyro drift $\Delta\mathrm{b}$. Hence, $\Delta\mathrm{q}$ is fed back to $\Delta\mathrm{b}$ thus $\Delta\dot{\mathrm{b}}$ is adaptive. This can improve the estimated precision of b and decrease the steady state error of $\Delta\mathrm{b}$. The analysis is as follows.

At time t, let the quaternion q represent the actual orientation of the rigid body with respect to the reference system, and corresponding rotation angle is Φ. Simultaneously, $\hat{\mathrm{q}}$ is the estimated quaternion and $\hat{\Phi}$ is the rotation angle. If the attitude is referred as a rotation, then attitude error is the rotation from actual attitude to estimated attitude, defined by

$$\Delta\mathrm{q} = \left[\cos\frac{\Delta\Phi}{2}\ \ E_x \sin\frac{\Delta\Phi}{2}\ \ E_y \sin\frac{\Delta\Phi}{2}\ \ E_z \sin\frac{\Delta\Phi}{2}\right]^{\mathrm{T}} \tag{21}$$

where $\Delta\Phi$ is the rotation angle derived from the rotation from q to $\hat{\mathrm{q}}$ about E axis, $\Delta\Phi \in [0,\ 2\pi)$; E_x, E_y, E_z are the components of unit vector of E expressed in the $Oxyz$ coordinate system.

If $\Delta q_1 = \cos\frac{\Delta\Phi}{2} > 0$, $\Delta\Phi \in (0,\ \pi)$, it is seen that $\hat{\mathrm{q}}$ advances q, that is, $\hat{\Phi} > \Phi$. The rotation is illustrated in Fig. 5(a).

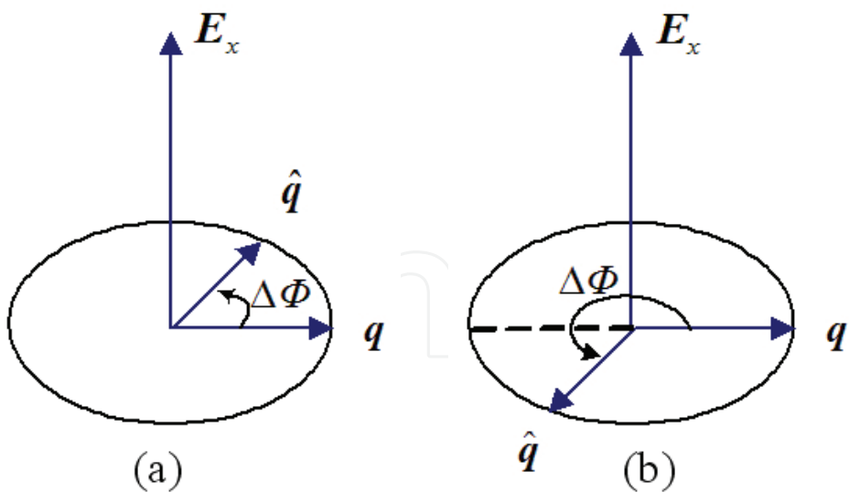


Fig. 5. The rotation of the error quaternion

We have $sign(\Delta q_1) = 1 > 0$, and the magnitude of $\Delta\dot{b}$ can be given by the product of scale factor $\frac{\alpha}{2}$ and Δq_{24}. If $\Delta q_1 = \cos\frac{\Delta\Phi}{2} < 0$, the results can be analogously analyzed.

Improved gyro model 2: The statistic mean of drift error Δb can be used for its estimate value, that is

$$\Delta \boldsymbol{b} = \mathrm{E}\left[\Delta \boldsymbol{b}(\mathrm{t_i})\right] \qquad t_i \in [t - \Delta \mathrm{T},\ t] \tag{22}$$

This model makes use of the noise distribution property of Δb in steady state and decreases the estimated error by the data processing. In this chapter, this model is applied in the Mode II of the following attitude determination scheme.

3.3 Filter implement

Based on the previous derivation, attitude determination scheme using EKF algorithm consists of state prediction and observation correction with the flow chart illustrated in Fig. 6.

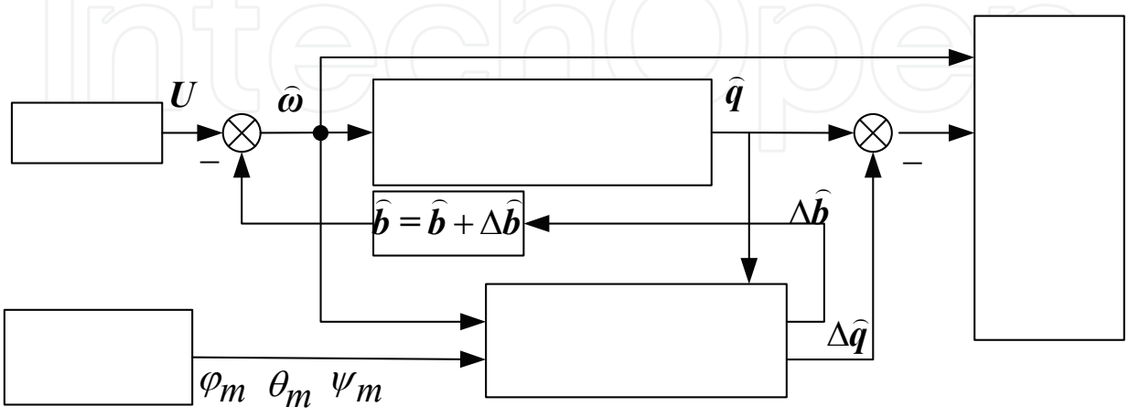


Fig. 6. The flow chart of attitude determination scheme

3.4 Simulation results

In this section, two types of mode of attitude determination system are used to estimate attitude. In each mode, we adopt different gyro drift model previously discussed. The following parameters are used for simulation.

The gyro "measurements" are simulated with a gyro noise standard deviation 0.1 deg/hr, a constant drift of 5 deg/hr, and measurement frequency of 50 HZ. The measurement error of star sensor is Gaussian white noise of 0.1 arcsec and measurement frequency is 5HZ. The measurements of infrared horizon senor are simulated with a constant bias of 0.1 deg, and Gaussian white noise of 0.05 deg and measurement frequency is 1 HZ.

3.4.1 Mode I

For the observation model 1 previous described, two types of gyro drift model are used in simulations. They are $\Delta\dot{b} = v_b$ (Traditional gyro model) and $\Delta\dot{b} = \frac{\alpha}{2} \cdot \Delta q_{24} \cdot sign(\Delta q_1) + v_b$ (Improved gyro model 1). The simulation results are shown as follows.

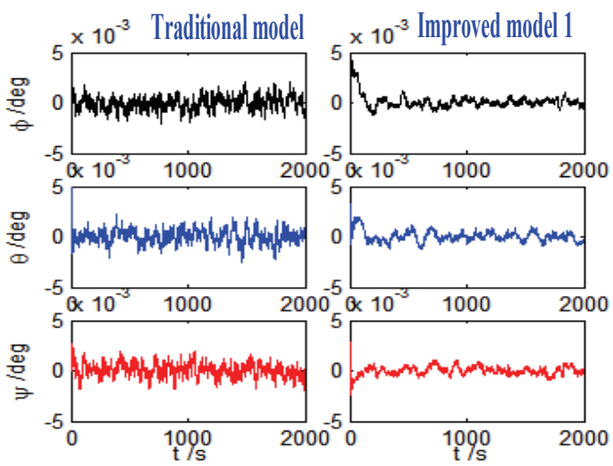


Fig. 7. Comparison of the attitude estimated error.

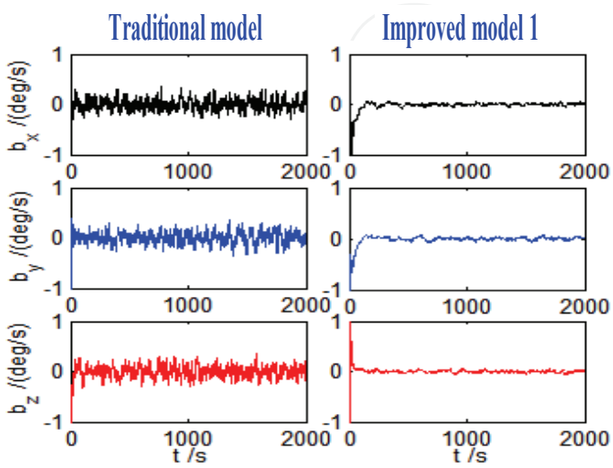


Fig. 8. Comparison of the gyro random drift estimated error.

		λ	b	ω
Traditional gyro model	Max	0.0024	0.4831	2.140e-4
	RMSx	7.251e-4	0.1089	4.109e-5
	RMSy	6.962e-4	0.1134	4.191e-5
	RMSz	6.498e-4	0.1027	3.983e-5
Improved gyro Model 1	Max	0.0018	0.2067	1.413e-4
	RMSx	4.147e-4	0.0238	2.849e-5
	RMSy	3.846e-4	0.0219	2.848e-5
	RMSz	4.304e-4	0.0249	2.860e-5

Table 3. Max and RMS of the stabilization estimate error(attitude unit: deg)

It is shown that the precision of the estimate of attitude and gyro drift increased dramatically when adopting improved gyro model 1. The attitude angular estimated error curves are smooth and the stability is enhanced. When adopting traditional gyro model, the attitude filter converged in 50 sec, but the estimated error is not stable; when adopting improved gyro model 1, the filter converged after a gap of 200 sec, but the estimated error is stable. Therefore, two types of gyro model can be integrated in use.

3.4.2 Mode II

For the observation model 2 previous described, two types of gyro drift model are used in simulations. They are $\Delta\dot{b} = v_b$ (Traditional gyro model) and $\Delta b = E[\Delta b(t_i)]$ (Improved gyro model 2). The simulation results are shown as follows.

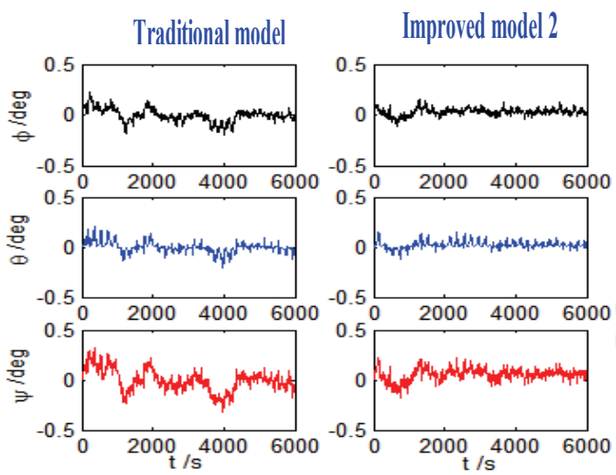


Fig. 9. Comparison of the attitude estimated error

From the Figs. 9-10 and Table 4, we can see that the precision of the estimate of attitude and gyro drift increased and the stability is enhanced when adopting improved gyro model 2. Theoretical analysis and simulation results indicate that the attitude determination system satisfies the design requirement and the improved gyro drift models are feasible and efficient.

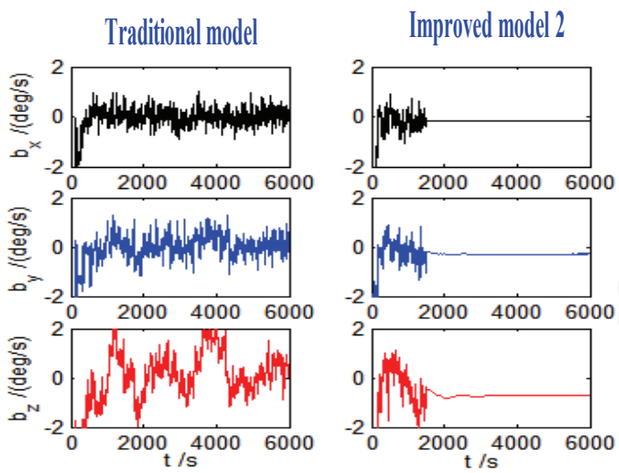


Fig. 10. Comparison of the gyro random drift estimated error

		λ	b	ω	φ_{bias} , θ_{bias}
Traditional gyro model	**Max**	0.3033	2.3769	7.280e-4	0.2825
	RMSx	0.0516	0.3759	1.080e-4	0.0587
	RMSy	0.0423	0.4179	1.194e-4	0.0533
	RMSz	0.0887	0.7534	2.112e-4	/
Improved gyro Model 2	**Max**	0.1527	0.1575	1.556e-4	0.0295
	RMSx	0.0219	0.1096	4.125e-5	0.0113
	RMSy	0.0202	0.0112	2.784e-5	0.0101
	RMSz	0.0393	0.0463	3.057e-5	/

Table 4. Max and RMS of the stabilization estimate error (attitude unit: deg)

4. Attitude control of three-axis stabilized spacecraft with momentum wheel system

Attitude control is the process of orienting the spacecraft in a specified or predetermined direction, which makes the spacecraft obtain the desired attitude angle and angular velocity. Attitude control in the large angle attitude maneuvers of spacecraft belongs to the tracking control area, and many mature control methods can be referred, e.g., classical control, adaptive control, robust control, prediction control, multimode control and intelligent control, et al. In this section, a key problem above control decoupling and precession inhibition for zero-bias-momentum spacecraft is discussed.

Although the angular momentum exchange device such as momentum wheel is widely applied to attitude control for three-axis stabilized spacecraft, further studies about control decoupling and precession inhibition are deficient. For example, when the satellite is controlled by the momentum wheel operated only in rate mode, it is known to decouple the roll and yaw channels for bias-momentum satellite. However, the decoupling is not usually carried out for zero-bias-momentum satellite, since three axes of it are usually assumed independent. In fact, if the momentum wheel operated only in rate mode, whatever the bias-momentum scheme or zero-bias-momentum scheme, the decoupling along roll and yaw channel must be carried out. Otherwise, there exists precession in both roll and yaw

directions. But in the actual practice, the decoupling is dispensablesince the control scheme includes magnetic control besides wheel control (Stickler & Alfriend, 1974). (Tian et al., 2001; Qian, 2002) analyze the ACS stability of spacecraft with angular momentum exchange device as actuator, and demonstrate that the introduction of magnetic unloading control can damp precession motion of the spacecraft effectively, which is the main reason why it is dispensable to decouple along roll and yaw channel. But in this way, the magnetic torque actuator is always required in work mode against the original design intention of the magnetic unloading system. Therefore, some researchers (Li et al., 2009) present a method to adjust the magnetic dipole moments along pitch axis to eliminate the precession and nutation, which is proved to be effective.

In this section, the principle which is used to eliminate precession and nutation for bias-momentum spacecraft is introduced to solve the attitude control problem for zero-bias-momentum spacecraft. Moreover, according to the differences between zero-bias-momentum scheme and bias-momentum scheme, the magnetic control command law has been improved to solve the precession inhibition problem effectively for zero-bias-momentum spacecraft.

4.1 Kinematic and dynamic model of attitude motion

4.1.1 Kinematic equation of motion

Based on the small-angle approximations, the linearized kinematic equation of motion of spacecraft can be given by (Wertz, 1998)

$$\boldsymbol{\omega} = \begin{bmatrix} \dot{\varphi} - \omega_0 \psi \\ \dot{\theta} - \omega_0 \\ \dot{\psi} + \omega_0 \varphi \end{bmatrix} \tag{23}$$

where $\boldsymbol{\omega}$ is the angular velocity of spacecraft with respect to inertial frame, ω_0 denotes the orbital angular velocity.

4.1.2 Dynamic equation of motion

Considering the rigid body model of spacecraft, the dynamic equation of motion of spacecraft equipped with momentum wheels as actuators is given by

$$\boldsymbol{I}\dot{\boldsymbol{\omega}} + [\boldsymbol{\omega}\times](\boldsymbol{I}\boldsymbol{\omega} + \boldsymbol{h}) = -\dot{\boldsymbol{h}} + \boldsymbol{T}_c + \boldsymbol{T}_d \tag{24}$$

Note that $\boldsymbol{H} = \boldsymbol{I}\boldsymbol{\omega}$ represents the angular momentum vector of spacecraft. $\boldsymbol{I}$ is the moment-of-inertia tensor; $\dot{\boldsymbol{h}}$ is the wheel control torque. $\boldsymbol{T}_c$ is the control torque which is not provided by the wheels and $\boldsymbol{T}_d$ is disturbance torque.

Substituting Eq.(23) into Eq.(24) yields the dynamic equations of motion with Euler angle representation given by

$$\begin{aligned} M_{dx} &= I_x\ddot{\varphi} + (I_y - I_x - I_z)\omega_0\dot{\psi} + (I_y - I_z)\omega_0^2\varphi + \\ &\quad I\dot{\Omega}_x + I\Omega_z(\dot{\theta} - \omega_0) - I\Omega_y(\dot{\psi} + \omega_0\varphi) \\ M_{dy} &= I_y\ddot{\theta} + I\dot{\Omega}_y + I\Omega_x(\dot{\psi} + \omega_0\varphi) - I\Omega_z(\dot{\varphi} - \omega_0\psi) \\ M_{dz} &= I_z\ddot{\psi} - (I_y - I_x - I_z)\omega_0\dot{\varphi} + (I_y - I_x)\omega_0^2\psi + \\ &\quad I\dot{\Omega}_z + I\Omega_y(\dot{\varphi} - \omega_0\psi) - I\Omega_x(\dot{\theta} - \omega_0) \end{aligned} \tag{25}$$

4.1.3 Disturbance torque

Since the environmental torques are not only related to the orbit, shape, and mass distribution of the spacecraft, but also solar activity, season, date and diurnal fluctuation, the calculations of environmental torques are very complicated. In the preliminary design, a Fourier expansion is usually used for disturbance torques expressed in the body frame of spacecraft with the consideration of the zero-order and one-order term. The orbital frequency ω_0 is chosen as the basic frequency of the harmonic term. Therefore, the disturbance torque model used in this chapter can be written as

$$\boldsymbol{T}_d = 10^{-3}\begin{bmatrix} 3\cos\omega_0 t + 1 \\ 1.5\sin\omega_0 t + 3\cos\omega_0 t \\ -3\sin\omega_0 t + 1 \end{bmatrix} \text{ (Nm)} \tag{26}$$

It is seen that the accumulated torque impulse arising from disturbance torque along pitch axis is zero. For small attitude angle, when the spacecraft orbits one circle, the accumulated impulse generated by the constant components of disturbance torque in the roll and yaw directions is approximately zero, while the accumulated impulse generated by the harmonic components are $\Delta H_X^I = 3T$ and $\Delta H_Z^I = 0$, respectively, where T is the orbital period.

4.2 Analysis of stability

Since the values of φ, θ, ψ and $\dot{\varphi}, \dot{\theta}, \dot{\psi}$ are very small, the linearization of the dynamic model can be given by

$$I_y\ddot{\theta} = -\dot{h}_y + T_{dy} \tag{27}$$

$$\begin{bmatrix} I_x s^2 + g_z\omega_0 & g_0 s \\ -g_0 s & I_z s^2 + g_x\omega_0 \end{bmatrix}\begin{bmatrix} \varphi \\ \psi \end{bmatrix} = -\begin{bmatrix} s & -\omega_0 \\ \omega_0 & s \end{bmatrix}\begin{bmatrix} h_x \\ h_z \end{bmatrix} + \begin{bmatrix} T_{cx} + T_{dx} \\ T_{cz} + T_{dz} \end{bmatrix} \tag{28}$$

It follows that

$$g_x = (I_y - I_x)\omega_0 - h_y,$$

$$g_z = (I_y - I_z)\omega_0 - h_y,$$

$$g_0 = (I_y - I_x - I_z)\omega_0 - h_y$$

From the above equations, we can see that the pitch axis loop is independent of roll and yaw axes and can be designed separately. There exists a close coupling along roll and pitch axis, and the coupling are different owing to the different control schemes. Consequently, the above attitude control is a nonlinear control problem which can be solved using two kinds of methods. One is to design the nonlinear control law for nonlinear problem, the other is to consider the coupling terms arising from the orbital frequency and angular momentum of wheels are small and assume the three channels are independent, so the control law can be designed separately.

In fact, if the spacecraft is controlled only by reaction wheels, whether the reaction wheels are operated in moment mode or momentum mode, the roll and yaw channels must be decoupled. Otherwise, the closed loop response of the system is a pure oscillation at an angular frequency of ω_0 . The analysis is as follows.

Consider the spacecraft is controlled with the wheels operated in rate mode and ignore the constant external disturbances. The linearized feedback control law along x axis and z axis is given by

$$\begin{bmatrix} V_X(s) \\ V_Z(s) \end{bmatrix} = \boldsymbol{G}_c(s) \begin{bmatrix} \varphi \\ \psi \end{bmatrix} \tag{29}$$

where $\boldsymbol{G}_c \in F^{2\times 2}$ is the transfer function, V_X and V_Z represent the control voltage of the reaction wheels along x axis and z axis, respectively.

Assume the initial attitude angle and angular velocity are zero, so we have

$$\begin{bmatrix} h_x \\ h_z \end{bmatrix} = \begin{bmatrix} \dfrac{K_r}{1+T_r} & 0 \\ 0 & \dfrac{K_r}{1+T_r} \end{bmatrix} \begin{bmatrix} V_x \\ V_z \end{bmatrix} \tag{30}$$

Substitute Eq.(30) into Eq.(24) and consider the spacecraft is controlled only by wheels, that is, $T_{cx} = T_{cz} = 0$, so we can obtain

$$\begin{bmatrix} I_x s^2 + g_z \omega_0 & g_0 s \\ -g_0 s & I_z s^2 + g_x \omega_0 \end{bmatrix} \begin{bmatrix} \varphi \\ \psi \end{bmatrix} = \begin{bmatrix} T_{dx} \\ T_{dz} \end{bmatrix} - \frac{K_r}{1+T_r s} \begin{bmatrix} s & -\omega_0 \\ \omega_0 & s \end{bmatrix} \boldsymbol{G}_c \begin{bmatrix} \varphi \\ \psi \end{bmatrix} \tag{31}$$

$$\begin{bmatrix} s & -\omega_0 \\ \omega_0 & s \end{bmatrix} \begin{bmatrix} I_x s & g_x \\ -g_z & I_z s \end{bmatrix} \begin{bmatrix} \varphi \\ \psi \end{bmatrix} = \begin{bmatrix} T_{dx} \\ T_{dz} \end{bmatrix} - \frac{K_r}{1+T_r s} \begin{bmatrix} s & -\omega_0 \\ \omega_0 & s \end{bmatrix} \boldsymbol{G}_c \begin{bmatrix} \varphi \\ \psi \end{bmatrix} \tag{32}$$

$$\begin{bmatrix} \varphi \\ \psi \end{bmatrix} = \frac{1}{s^2+\omega_0^2} \left(\begin{bmatrix} I_x s & g_x \\ -g_z & I_z s \end{bmatrix} + \boldsymbol{G}_c \frac{K_r}{1+T_r s} \right)^{-1} \begin{bmatrix} s & \omega_0 \\ -\omega_0 & s \end{bmatrix} \begin{bmatrix} \varphi \\ \psi \end{bmatrix} \begin{bmatrix} T_{dx} \\ T_{dz} \end{bmatrix} \tag{33}$$

It is obvious that no matter what the forms of $\boldsymbol{G}_c$ is, $s = \pm j\omega_0$ are always a couple of poles of the closed loop system. However, $s = \pm j\omega_0$ are the uncontrolled modality of the system, and the system always oscillate with the angular frequency ω_0 , that is, there exists precession in both roll and yaw directions. Therefore, it is imperative to introduce some other controls to eliminate the above precession for the zero-bias-momentum spacecraft.

4.3 Principle of magnetic control

For the precession inhibition problem without decoupling, (Tian et al., 2001; Qian, 2002) demonstrated that the introduction of magnetic unloading control can damp spacecraft precession effectively. But the magnetic actuator is always required in work mode against the original design intention of the magnetic unloading system. (Li et al., 2009) presents a method to adjust the magnetic dipole moments along pitch axis to eliminate the precession

and nutation for three-axis stabilized spacecraft. In this section, we introduce the principle that how to eliminate precession and nutation used in bias-momentum wheel spacecraft and improve the magnetic control law.

Precession control and nutation damping are provided by driving the pitch dipole according to

$$M_y = -K_1 B_x \varphi - K_2 B_z \psi + m_y - K_3 \dot{B}_y \tag{34}$$

where φ and ψ represent the corresponding deviation of roll and yaw angle from the command attitude, respectively; B represents magnetic field intensity; $\dot{B}_y$ is derived from the differential of the magnetometer aligned along y axis; m_y is the magnetic moment used to eliminate precession, and K_1, K_2, K_3 are the gains. The discussion below demonstrated that the prior three terms provide precession control and the last one nutation damping.

4.3.1 Nutation damping

For small attitude errors, we have

$$\dot{B}_y = B_z \dot{\varphi} - B_x \dot{\psi} \tag{35}$$

Control torques caused by the nutation damping term ($-K_3 \dot{B}_y$) in Eq.(34) are given by

$$\begin{aligned} T_{Mx} &= -K_3 \dot{B}_y B_z = -K_3 B_z^2 \dot{\varphi} + K_3 B_x B_z \dot{\psi} \\ T_{Mz} &= -K_3 \dot{B}_y B_x = -K_3 B_x^2 \dot{\psi} + K_3 B_x B_z \dot{\varphi} \end{aligned} \tag{36}$$

The first term on the right-hand-side indicates the damping torque is proportional to the nutational amplitude. The pitch component of the magnetic field intensity generally varies small, whereas the value of $\dot{B}_y$ is somewhat larger when the spacecraft performs the nutational cone motion, which can generate the damping torques together with geomagnetic field.

4.3.2 Precession control

Ignore the related term associated with the moment of inertia and consider the coupling term associated with orbital motion solely. The precession equations of motion are given by

$$\begin{aligned} \omega_0 h_y \varphi + h_y \dot{\psi} - h_z \omega_0 &= T_{cx} \\ -h_y \dot{\varphi} + \omega_0 h_y \psi + h_x \omega_0 &= T_{cz} \end{aligned} \tag{37}$$

For bias-momentum spacecraft, we have inequalities $h_y >> h_x$ and $h_y >> h_z$, so the precessional effects generated by h_x and h_z with respect to by h_y are small quantity, which can be ignored. However, h_x, h_y, h_z are all small quantities for zero-bias-momentum spacecraft. The method used in bias-momentum spacecraft can be used in zero-bias-momentum spacecraft to eliminate the precession results from quantity h_y, but falls short in the precession arising from $h_x \omega_0$ and $h_z \omega_0$. It can be further seen from the simulation results below that the magnetic actuator can weaken the precession amplitude dramatically but there still exists precession. Accordingly, momentum moment of reaction wheels referred as feedback signal is introduced to magnetic torque, which eliminates the precession arising from h_x and h_z effectively. Simulation results verify the feasibility of the scheme.

1. Elimination of precession caused by h_y

Assume the magnetic dipole moment is adopted in the similar form used in bias-momentum spacecraft, that is

$$M_{y1} = -K_1 B_x \varphi - K_2 B_z \psi \tag{38}$$

and the generated magnetic torque can be given by

$$T_1 = M_1 \times B = \begin{bmatrix} 0 \\ M_{y1} \\ 0 \end{bmatrix} \times \begin{bmatrix} B_x \\ B_y \\ B_z \end{bmatrix} = \begin{bmatrix} -K_1 B_x B_z \varphi - K_2 B_z^2 \psi \\ 0 \\ K_1 B_x^2 \varphi + K_2 B_x B_z \psi \end{bmatrix} \tag{39}$$

it can be changed to

$$\begin{bmatrix} T_{cx1} \\ T_{cz1} \end{bmatrix} = \begin{bmatrix} -K_1 B_x B_z & -K_2 B_z^2 \\ K_1 B_x^2 & K_2 B_x B_z \end{bmatrix} \begin{bmatrix} \varphi \\ \psi \end{bmatrix} = \begin{bmatrix} -k_1 & -k_2 \\ k_3 & k_4 \end{bmatrix} \begin{bmatrix} \varphi \\ \psi \end{bmatrix} \tag{40}$$

with

$$\begin{aligned} k_1 &= K_1 B_x B_z \quad & k_2 &= K_2 B_z^2 \\ k_3 &= K_1 B_x^2 \quad & k_4 &= K_2 B_x B_z \end{aligned} \tag{41}$$

The percession equations of motion results from h_y via Eq.(37) can be given by

$$\begin{aligned} -h_y(\dot{\psi} + \omega_0 \varphi) &= T_{cx1} \\ h_y(\dot{\varphi} - \omega_0 \psi) &= T_{cz1} \end{aligned} \tag{42}$$

which can be rewritten as

$$\begin{bmatrix} -\omega_0 h_y & -s h_y \\ s h_y & -\omega_0 h_y \end{bmatrix} \begin{bmatrix} \varphi \\ \psi \end{bmatrix} = \begin{bmatrix} T_{cx1} \\ T_{cz1} \end{bmatrix} \tag{43}$$

Combining Eq.(40) gives

$$\begin{bmatrix} \omega_0 h_y - k_1 & s h_y - k_2 \\ -s h_y + k_3 & \omega_0 h_y + k_4 \end{bmatrix} \begin{bmatrix} \varphi \\ \psi \end{bmatrix} = 0 \tag{44}$$

The characteristic equation of the system is given by

$$C(s) = s^2 h_y^2 - h_y(k_2 + k_3)s + k_2 k_3 - k_1 k_4 + (k_4 - k_1)\omega_0 h_y + \omega_0^2 h_y^2 = 0 \tag{45}$$

For bias-momentum spacecraft, we have $h_y < 0$, but for zero-bias-momentum spacecraft the value of h_y can be a positive or negative, different from the one of bias-momentum spacecraft. By the Routh criterion, one finds that the stability requirements are

$$-h_y(k_2+k_3)>0 \tag{46}$$

$$k_2k_3-k_1k_4+(k_4-k_1)\omega_0h_y+\omega_0^2h_y^2>0 \tag{47}$$

We can find the identity $k_2k_3=k_1k_4$ via Eq.(41). If we set $K_1=K_2$ in Eq.(41), thus we can obtain $k_1=k_4$ and Eq.(47) can be reduced to $\omega_0^2h_y^2>0$, which satisfies the stability condition. Furthermore, substituting k_2 and k_3 into Eq.(46) gives

$$-h_y(K_1B_x^2+K_2B_z^2)>0 \tag{48}$$

Together with the equality $K_1=K_2$ leads to

$$-h_yK_1(B_x^2+B_z^2)>0 \tag{49}$$

so

$$h_yK_1<0 \tag{50}$$

Therefore, the sign of K_1 can be determined by $-sign(h_y)$ and the magnitude of it can be computed by the performance indices of second-order system $C(s)$, where $sign(\bullet)$ is sign function.

2. Elimination of precession caused by h_x and h_z

It is known from the previous analysis that the method used in bias-momentum spacecraft to eliminate precession can't weaken the precession terms of $-h_z\omega_0$ and $h_x\omega_0$. To solve this problem, the approach that adding the additional magnetic dipole moment along pitch axis is presented. Suppose m_y is that magnetic moment, and using the relation $T_{m1}=m_y\times B$ we can obtain

$$\begin{aligned} T_{mx1}&=m_yB_z\\ T_{mz1}&=-m_yB_x \end{aligned} \tag{51}$$

The value of m_y can be determined by minimizing the following function

$$J=\left[m_yB_z-(-h_z\omega_0)\right]^2+\left[-m_yB_x-(h_x\omega_0)\right]^2 \tag{52}$$

Setting $\partial J/\partial m_y=0$ leads to

$$2m_yB_z^2+2B_zh_z\omega_0+2m_yB_x^2+2B_xh_x\omega_0=0 \tag{53}$$

from which we have

$$m_y=-\frac{(B_xh_x+B_zh_z)}{B_x^2+B_z^2}\omega_0 \tag{54}$$

4.3.3 Magnetic dipole moment

According to the previous analysis, the control torque to eliminate the precession can be given by

$$T = T_1 + T_{m1} = \begin{bmatrix} -K_1 B_x B_z \varphi - K_2 B_z^2 \psi + m_y B_z \\ K_1 B_x^2 \varphi + K_2 B_x B_z \psi - m_y B_x \end{bmatrix} \tag{55}$$

and the corresponding command acting on the pitch axis is

$$M_y = M_{y1} + m_y = -K_1 (B_x \varphi + B_z \psi) + m_y \tag{56}$$

So the magnetic dipole moment along pitch axis can be obtained by

$$M_y = -K_1 (B_x \varphi + B_z \psi) - K_3 \dot{B}_y + m_y \tag{57}$$

which is in agreement with Eq.(34).

4.4 Simulation results

The feasibility of the proposed scheme is verified by the numerical simulations. The PID control law is adopted in the zero-bias-momentum spacecraft and the following parameters are used in simulations.

In accord with the previously stated assumptions regarding the geomagnetic field and orbit, we have

$$\begin{cases} B_x = B_0 \cos u \\ B_y = 0 \\ B_z = 2B_0 \sin u \end{cases}$$

where $B_0 = 10^{-2}(\mathrm{T})$ is the equatorial magnetic field intensity, and $u = \omega_0 t$ is the orbit argument, measured from ascending node. The spacecraft's moment of inertia tensor is

$$\boldsymbol{I} = \begin{bmatrix} 4229.8 & 48.9 & 1.1 \\ 48.9 & 1458.2 & 252.6 \\ 1.1 & 252.6 & 4450.6 \end{bmatrix} (\mathrm{kg \cdot m^2})$$

The parameters of PID control law are $\boldsymbol{K}_p = 3 \times 10^{-3} \cdot diag(\boldsymbol{I})$, $\boldsymbol{K}_d = 7.36 \times 10^{-2} \cdot diag(\boldsymbol{I})$ and $\boldsymbol{K}_I = 1 \times 10^{-5} \cdot diag(\boldsymbol{I})$, respectively. The orbital angular velocity is $\omega_0 = 0.001(\mathrm{rad/s})$. The initial states are set as $\varphi_0 = \theta_0 = \psi_0 = 0.5^\circ$, and $\boldsymbol{\omega} = \begin{bmatrix} 0.04 & -0.08 & 0.04 \end{bmatrix}^{\mathrm{T}} (\mathrm{rad/s})$. The gains are chosen as $K_1 = K_2 = 8.2 \times 10^4$ and $K_4 = 10$.

4.4.1 Case 1

Consider the PID control law is solely adopted for the zero-bias-momentum spacecraft. The simulation results are shown as Fig. 11. It is shown that the attitude and wheel speed oscillate with frequency ω_0, which agrees well with the preceding stability analysis. The amplitude of attitude is 0.5°, and the curves of attitude and wheel speed in both roll and yaw directions diverge. Therefore, the additional control torque is required to eliminate precession and nutation for the ACS since PID control law doesn't work well.

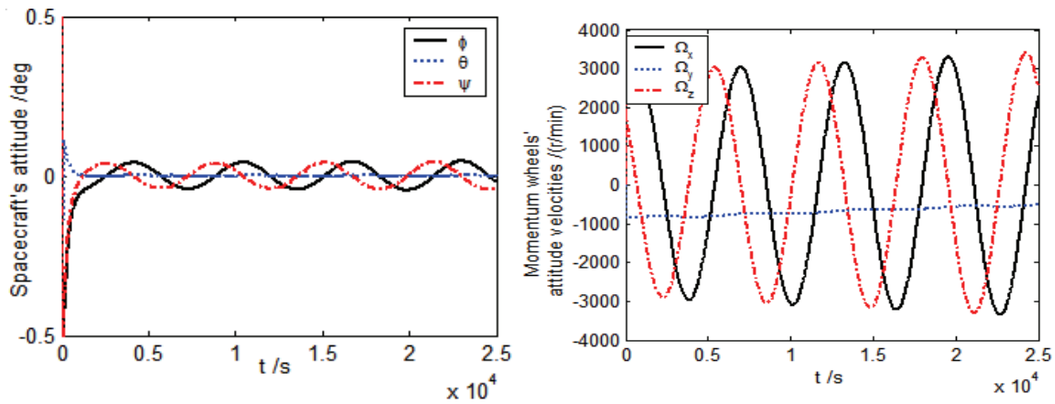


Fig. 11. Spacecraft's attitude and wheel speed versus time (PID)

4.4.2 Case 2

On the basis of Case 1, the method for eliminating precession and nutation used in the bias-momentum system is introduced to zero-bias-momentum system, that is, we use the magnetic dipole moment along pitch axis, $M_y = -K_1 B_x \varphi - K_2 B_z - K_3 \dot{B}_y$. As can be seen in Fig. 12, the attitude can converge quickly and the precession effect is weakened. But from the wheel speed curve, we can see that the precession is not wholly eliminated and still oscillates periodically.

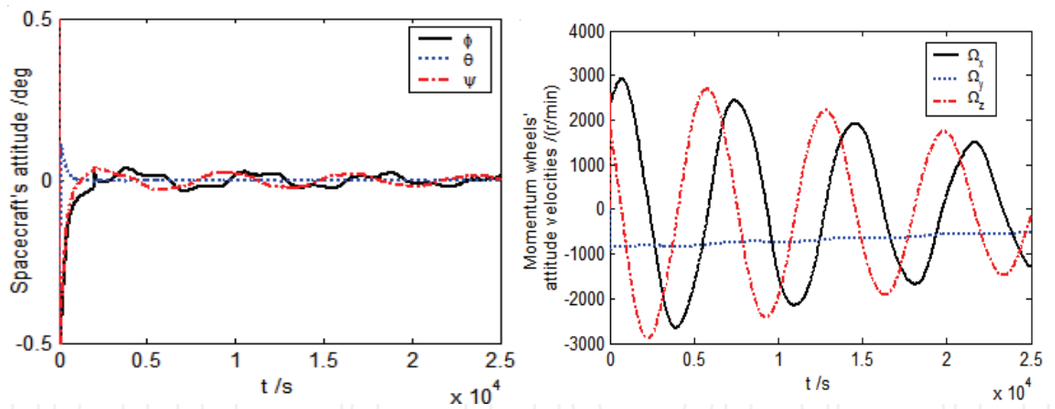


Fig. 12. Spacecraft's attitude and wheel speed versus time (Magnetic Unloading Control)

4.4.3 Case 3

The precession caused by h_x and h_z is further studied in this case. m_y is introduced into the pitch magnetic dipole moment, that is, $M_y = -K_1 B_x \varphi - K_2 B_z \psi + m_y - K_3 \dot{B}_y$. The simulation results are given in Fig.13. Compared with the previous cases, the convergence of attitude is better and attitude accuracy in steady state is higher. From the wheel speed curve we can see the effect of precession is basically eliminated, and the wheel speeds in three axes are stabilized at the neighborhood of corresponding fixed value. It is shown that the selected magnetic torque can be used to eliminate precession effectively, satisfying the attitude stabilization requirements of zero-bias-momentum system.

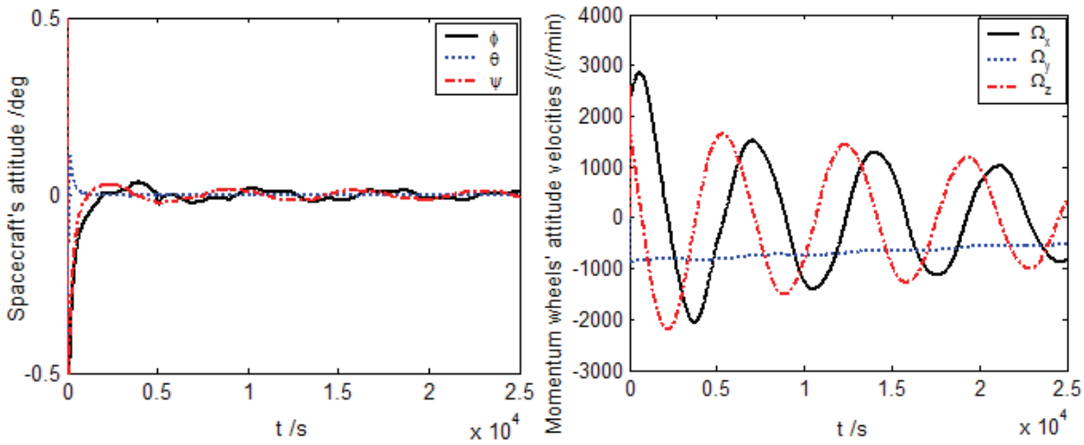


Fig. 13. Spacecraft's attitude and wheel speed versus time (Precession Control)

5. Conclusion

In this chapter, the three key techniques involved guidance, navigation and control are investigated. The method using NLP method to solve MEMCP is improved and a new construction method for initial feasible solution of the NLP is presented. The improved approach makes the initial attitude trajectory approach the actual one and improves the computational efficiency. For the attitude determination system, two types of improved gyro-drift models are presented. Simulation results show that the improved models can decrease the steady state deviation of estimated errors and improve the estimated accuracy. In the section 4, a key problem above control decoupling and precession inhibition for zero-bias-momentum spacecraft is discussed. The principle used to eliminate precession and nutation for bias-momentum spacecraft is introduced to solve the attitude control problem for zero-bias-momentum spacecraft. According to the differences between zero-bias-momentum scheme and bias-momentum scheme, the magnetic control command law has been improved to solve the precession inhibition problem effectively for zero-bias-momentum spacecraft.

6. Reference

Chung, T. S. & Wu, C. J. (1992). A computationally efficient numerical algorithm for the minimum-time control problem of continuous systems. *Automatica*, Vol.28, pp. 841-847

Dwyer, T. A. W. (1982). The control of angular momentum for asymmetric rigid bodies. IEEE Trans. *Autom.Control*, Vol.3, pp.686-688

Junkins, J. L & Turner, J. D. (1980). Optimal continuous torque attitude maneuvers. *Journals of Guidance, Control, Dynamics*, Vol 3(3), pp. 210-217

Li, P.K., Qian, S., Guo, C.F. & Cai, H. (2009). Research on satellite attitude control problems of zero-momentum reaction wheel system, *Chinese Space Science and Technology*, Vol.29(2), pp.25-32

Li, F. & Bainum, P.M. (1994). Numerical approach for solving rigid spacecraft minimum time attitude maneuvers. *Journals of Guidance, Control, Dynamics*, Vol 13 (1), pp. 38-45

Qian, Y. (2002). High accuracy attitude determination and control system for the three-axis stabilized satellite. Northwestern Polytechnical University, Dr Thesis

Qian, S., Li, P. K., Zhang, S. F. & Cai, H. (2009). Satellite attitude estimation based on improved model of the gyro random drift, *Journal of Astronautics*, Vol.30(2), pp.585-589

Schaub, H. & Junkins, J. L. (1997). New penalty functions and optimal control formulation for spacecraft attitude control problems. *Guidance Control Dyn*, Vol.20(3), pp.428-434

Stickler, A. C. & Alfriend, K. T. (1974). An Elementary Magnetic Attitude Control System. *AIAA paper*, No.74-923

Tian, C. H., Ma, G. F., Li, C. J., et al. (2001). General problems of satellite attitude control. *Techniques of Automation and Applications*, No.1, pp.9-12

Thienel, J. K. (2004). Nonlinear observer/controller designs for spacecraft attitude control systems with uncalibrated gyros. Department of Aerospace Engineering, *Dr Thesis*

Vadali, S. R. & Junkins, J. L. (1984). Optimal open-loop and stable feedback control of rigid spacecraft attitude maneuvers. *Astronaut Sci*, Vol.32:pp.105-122

Vadali, S. R. & Junkins, J. L. (1983). Spacecraft large angle rotational maneuvers with optimal momentum transfer. *Astronaut Sci*, Vol.31, pp. 217-235

Wertz, J. R. ed. (1998). *Spacecraft Attitude Determination and Control*, Kluwer Academic, Dordrecht, The Netherlands

Wang, J. Q. (2004). Research for satellite autonomous navigation and fusion attitude determination algorithm based on attitude sensors. Harbin Institute of Technology, *Dr Thesis*, pp.90-96

Yang, C. C., Li, C. L. & Wu, C. J. (2007). Minimal energy maneuvering control of a rigid spacecraft with momentum transfer. *Journal of the Franklin Institute*, *ScienceDirect,* pp.991-1005

Zhang, S. F., Qian, S. & Li, P. K. (2009). Study on the minimal energy maneuvering control of a rigid spacecraft with momentum transfer, *Journal of Astronautics*, Vol.30(4), pp.1504-1509



Advances in Spacecraft Technologies

Edited by Dr Jason Hall

ISBN 978-953-307-551-8
Hard cover, 596 pages
Publisher InTech
Published online 14, February, 2011
Published in print edition February, 2011

The development and launch of the first artificial satellite Sputnik more than five decades ago propelled both the scientific and engineering communities to new heights as they worked together to develop novel solutions to the challenges of spacecraft system design. This symbiotic relationship has brought significant technological advances that have enabled the design of systems that can withstand the rigors of space while providing valuable space-based services. With its 26 chapters divided into three sections, this book brings together critical contributions from renowned international researchers to provide an outstanding survey of recent advances in spacecraft technologies. The first section includes nine chapters that focus on innovative hardware technologies while the next section is comprised of seven chapters that center on cutting-edge state estimation techniques. The final section contains eleven chapters that present a series of novel control methods for spacecraft orbit and attitude control.

How to reference

In order to correctly reference this scholarly work, feel free to copy and paste the following:

Shifeng Zhang, Shan Qian and Lijun Zhang (2011). Optimal Control Techniques for Spacecraft Attitude Maneuvers, Advances in Spacecraft Technologies, Dr Jason Hall (Ed.), ISBN: 978-953-307-551-8, InTech, Available from: http://www.intechopen.com/books/advances-in-spacecraft-technologies/optimal-control-techniques-for-spacecraft-attitude-maneuvers

INTECH
open science | open minds

InTech Europe
University Campus STeP Ri
Slavka Krautzeka 83/A
51000 Rijeka, Croatia
Phone: +385 (51) 770 447
Fax: +385 (51) 686 166
www.intechopen.com

InTech China
Unit 405, Office Block, Hotel Equatorial Shanghai
No.65, Yan An Road (West), Shanghai, 200040, China
中国上海市延安西路65号上海国际贵都大饭店办公楼405单元
Phone: +86-21-62489820
Fax: +86-21-62489821

© 2011 The Author(s). Licensee IntechOpen. This chapter is distributed under the terms of the Creative Commons Attribution-NonCommercial-ShareAlike-3.0 License, which permits use, distribution and reproduction for non-commercial purposes, provided the original is properly cited and derivative works building on this content are distributed under the same license.

IntechOpen

IntechOpen